Proceedings of the ASME 2024 Conference on Smart Materials, Adaptive Structures and Intelligent Systems SMASIS 2024 September 9-11, 2024, Atlanta, GA, USA, USA

# SMASIS2024-139941

## KALIMBA INSPIRED METASTRUCTURE FOR FREQUENCY SELECTIVITY

Hrishikesh Gosavi; Evelyn James, Rachel Cole, Vijaya V N Sriram Malladi
VITAL Structures Group,
Department of Mechanical Engineering-Engineering Mechanics
Michigan Technological University
Houghton, Michigan, 49931

#### **ABSTRACT**

In this study, the frequency selectivity phenomenon in the mammalian cochlea is replicated in a simulated environment. Frequency selectivity is found to be of crucial importance in the accurate perception of environmental noise. Previous studies have found that mammalian cochlea consists of basilar membrane which varies in width and stiffness along its length. This results in a gradient in mechanical properties and in turn results in a place-coding mechanism, where different frequencies of sound cause maximum displacement of the basilar membrane at specific locations along its length. The basilar membrane consists of multiple hair cells located along its length. The displacement of the basilar membrane due to sound waves causes hair cells to bend. This bending of hair cells activates ion channels, leading to the generation of electrical signals. Leveraging the principles of cochlear processing, a Kalimba-key-based broadband vibroacoustic device is developed in this study having potential implications for sensory technology and human perception enhancement. Dynamic vibration resonators (DVRs) are employed in this research to emulate the frequency-selective behavior of the mammalian cochlea where the DVRs act as hair cells. A beam structure, acting as a platform for 136 strategically placed DVRs, each corresponding to a Kalimba instrument key is considered. Upon stimulation, these Kalimba keys replicate the vibrations of the cochlear basilar membrane, enabling the recreation of frequency selectivity across a broad spectrum. To simulate the system, a Timoshenko beam is considered to consist

of spatially attached Kalimba keys modeled as a Single-Degree Of Freedom (SDOF) systems. A Finite Element (FE) model of this system is developed to calculate the response of the system. Frequency selectivity for different combinations of Kalimba keys is explored in this study. This study shows promising results having potential implications extending beyond healthcare, encompassing fields such as robotics where the integration of biological cochlear principles could enhance robots' sensory perception and interaction capabilities in diverse environments

#### 1 INTRODUCTION

The study and modeling of the behavior of cochlea have been of great interest to researchers as this organ is of crucial importance in auditory processing. This research has enabled the development of cochlear implants, providing hearing restoration. The cochlea plays an important role in auditory processing through frequency selectivity, allowing the discrimination of different frequencies within the auditory environment [1]. This frequency selectivity is primarily achieved through the cochlear organ corti which lies on top of the basilar membrane (BM) [2]. This BM consists of auditory sensor cells along its length, also called 'hair cells' [3]. The cochlea's tonotopic organization, where different frequencies are mapped along its length, is maintained by the arrangement and sensitivity of hair cells. These hair cells convert mechanical vibrations caused by incoming sound waves into electrical signals which are interpreted by the brain. Different hair cells are tuned to respond preferentially to specific

<sup>\*</sup>Address all correspondence to this author.

frequencies, allowing for the discrimination of different pitches or tones and analyzing complex auditory signals.

Several factors including exposure to loud noise, aging, and genetic disorders can cause irreversible damage to hair cells [4]. To overcome the hearing loss caused by this damage, cochlear implants are a widely accepted solution that bypass the damaged hair cells and directly stimulate the auditory nerve fibers with electrical signals. Considerable work has been done in developing cochlear implants for several listening situations. A review of this can be found in [5, 6]. Although cochlear implants are effective, they are prone to certain limitations such as high cost, error-prone electrode placement, limited compatibility with different types of hearing loss, and requirement of surgical procedure for installation [7]. Artificial Basilar Membranes (ABM) are effective alternatives that overcome the limitations of cochlear implants by providing improved frequency selectivity, and the potential for better integration with cochlear tissues [8]. ABMs mimic the frequency selectivity function of the natural basilar membrane in the cochlea by utilizing techniques such as microelectromechanical systems (MEMS) [9]. The design of ABMs involves two considerations, mechanical frequency selectivity and acoustic-to-electrical energy conversion [10]. The acoustical to electrical energy conversion is achieved by utilizing piezoelectric/piezoresistive effects [11, 12, 13, 14], optical measurements [15, 16], and triboelectric effects [16]. Considerable work has been done in this domain and summarized in [10].

ABMs have mechanical components whose structural parameters can be altered to ensure frequency selectivity. Von Békésy proposed a model for ABM for the first time that consisted of two cylinders with a pre-stretched membrane clamped between them [17, 18]. Following this, multiple studies were done to manufacture cochlear models by Chadwick et al [19], and several others [20, 21]. White and Grosh [22] developed a fluid-filled variable impedance wave-guide using micromachining. However, the longitudinal stiffness of the basilar membrane is entirely neglected in this work resulting in a compromise in filtering quality. A widespread approach to developing ABM has been to use an array of beams having different natural frequencies. This variation of natural frequencies results in frequency selectivity. Tanaka et al [23] proposed for the first time a 'fishbone' type mechanical cochlea replicating the resonator array structure of a fishbone. Following this, multiple groups have developed ABMs based on beam array structure. Shintaku et al [24] fabricated a micro-beam array having a varying thickness and analyzed the effect of altering the thickness on the frequency selectivity of the ABM. However, accurate control of thickness can be difficult to achieve from a manufacturing perspective. As against this, multiple studies have been done in developing ABM wherein the natural frequency variation in beam arrays is achieved by altering the lengths of the beams. Kim et al [25] developed an ABM which consisted of 10 beams having lengths in the range  $1140-3300 \mu m$ . The frequency selectivity of the ABM was analyzed using piezoelectric output. [12] have mimicked the frequency selectivity using micromechanical cantilever arrays. Jeon et al [26] characterized the behavior of Piezoelectric Aluminum-Nitride Beam Array in air and fluid. A detailed review of developments in beam array type ABMs can be found in [10].

As the traditional approach to using beam-type arrays for ABMs involves complex fabrication and assembly, it has limited tunability and versatility. To overcome these limitations, a novel design based on a locally resonant metastructure is proposed in this study. Metastructures are periodic structures that inhibit wave propagation within specific frequency ranges known as 'bandgaps'. A locally resonant metastructure consists of a host structure consisting of periodically repeating resonances [27]. Considerable work has been done in studying the characteristics of a locally resonant metastructure consisting of a beam as a host structure to which local resonances are attached. The local resonances can be designed and manufactured in several ways. [28] utilized 3D printed oscillators as local resonances while double cantilever beam resonators were used in [29]. Chavan et al [30] utilized dynamic vibrational resonators (DVRs) as local resonances. The DVRs consisted of beams having a tip mass attached. Other works related to locally resonant beams can be found in [31]. Inspiring from the beam array ABMs and locally resonant metastructures, a design for ABM is proposed in this study which consists of a host beam to which keys from the well-known Kalimba instrument are attached as resonators. This locally resonant metastructure results in bandgaps, thus exhibiting frequency selectivity by inhibiting wave propagation in the bandgap frequency region. The bandgap region is identified by calculating the Frequency Response Function (FRF) and locating the frequency range characterized by a significant drop in the amplitude and is void of natural frequencies. Since the Kalimba keys are tuned to a particular frequency (of a musical note), the keys attached to the beam act as hair cells attached to BM, replicating the cochlear behavior. In this simulation study, multiple keys are attached spatially through the length of the host beam. A set of keys tuned to a musical note is considered. Multiple such sets each tuned to a different musical note are attached to the beam and frequency selectivity is studied. Each key is approximated as a Single-Degree-of-Freedom (SDOF) system and multiple SDOF systems are attached to the beam.

The paper is structured as follows. The Finite Element (FE) formulation of the host beam is discussed in the following section. Subsequently, the SDOF formulation of keys is discussed. Following this, the bandgap frequency range and frequency selectivity based on different types of keys are studied. Lastly, the paper concludes by discussing the results and scope of the future work.

#### 2 HOST BEAM FE FORMULATION

To develop a macro-scaled model, a beam of aluminum 6061-T6 material having a cross-section of the length of 12 ft having a thickness of 0.25 inches and width of 1 inch is considered in this study. A Timoshenko beam formulation is considered. The Timoshenko beam equation is given as [32],

$$GA\kappa\left(\frac{\partial \psi(x,t)}{\partial x} - \frac{\partial^2 y(x,t)}{\partial x^2}\right) + \rho A \frac{\partial^2 y(x,t)}{\partial t^2} = q(x,t), \quad (1)$$

$$GA\kappa\left(\frac{\partial y(x,t)}{\partial x} - \psi(x,t)\right) + EI\frac{\partial^2 \psi(x,t)}{\partial x^2} = \rho I\frac{\partial^2 \psi(x,t)}{\partial t^2}, \quad (2)$$

where G is the shear modulus  $(N/m^2)$ , A is the area of cross-section  $(m^2)$ , y(x,t) and  $\psi(x,t)$  are the transverse displacement (m) and the angle of rotation (rad) at location x (m) and time t (s), q is the load (N), E is the Young's Modulus  $(N/m^2)$ ,  $\rho$  is the density  $(kg/m^3)$ , and I  $(kgm^2)$  is the moment of inertia. From Eqs. (1) and (2) finite element model is developed by discretizing the beam into second-order shape functions and formulating the mass and stiffness matrices of the beam. The frequency of the highest note in the considered keys) and a convergence test was performed wherein the change in the natural frequencies of the beam was observed by increasing the number of elements. This change was quantified in terms of the  $L_2$  norm. Figure 1

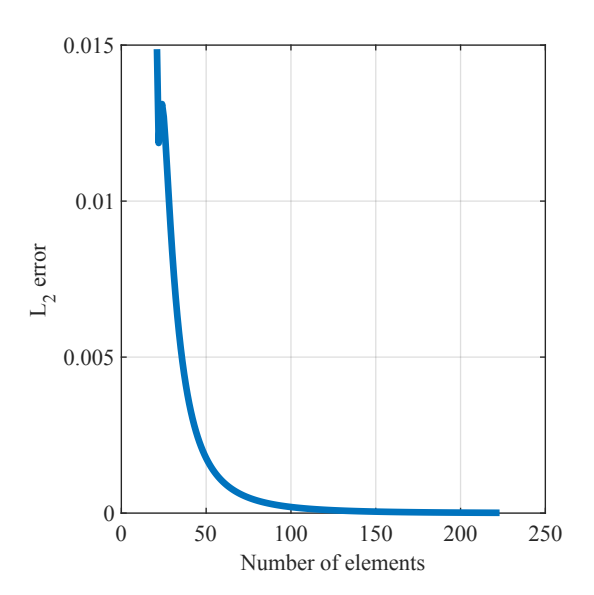


**FIGURE 1**. FE model of the host beam was found to converge at 223 finite elements

shows the change of natural frequencies with respect to the in-

crease in the number of elements. From Figure 1 it can be said the FE model converged for 223 elements. Using 223 elements, the mass  $\mathbf{M} \in \mathbb{R}^{(894 \times 894)}$  and the stiffness  $\mathbf{K} \in \mathbb{R}^{(894 \times 894)}$  matrices were formulated. Readers are referred to [30] for a detailed derivation of mass and stiffness matrices from Eqs. (1) and (2).

The governing equation of motion of the beam can be given as,

$$\mathbf{M}\ddot{\mathbf{x}} + \mathbf{C}\dot{\mathbf{x}} + \mathbf{K}\mathbf{x} = \mathbf{f}(\mathbf{t}),\tag{3}$$

where C is the damping matrix, x the vector of co-ordinates of the nodes and f(t) is the harmonic input force. Assuming a proportional damping model, the damping matrix is given as,

$$\mathbf{C} = \alpha \mathbf{M} + \beta \mathbf{K}. \tag{4}$$

The coefficients  $\alpha$  and  $\beta$  were assumed to be  $\alpha = 1 \times 10^{-5}$  and  $\alpha = 1 \times 10^{-6}$ . The FE model of the beam was formulated in MATLAB. The FE formulation of the beam given by Eq. (3) will be considered as the basis of the addition of Kalimba key resonators in the subsequent sections. The FE formulation given by Eq. (3) is used for the FRF of the beam and later of the metastructure. To calculate the FRF, consider the Laplace transform of Eq. (3)

$$\mathcal{L}(\mathbf{M}\ddot{\mathbf{x}} + \mathbf{C}\dot{\mathbf{x}} + \mathbf{K}\mathbf{x}) = \mathcal{L}(\mathbf{f}(\mathbf{t})). \tag{5}$$

Which becomes,

$$(\mathbf{M}s^2 + \mathbf{C}s + \mathbf{K})\mathbf{X}(s) = \mathbf{F}(s). \tag{6}$$

Putting  $s = j\omega$ , where  $\omega$  is the frequency in rad/s,

$$(-\omega^2 \mathbf{M} + j\omega \mathbf{C} + \mathbf{K})\mathbf{X}(\omega) = \mathbf{F}(\omega). \tag{7}$$

The FRF is then given as,

$$\mathbf{X}(\boldsymbol{\omega}) = (-\boldsymbol{\omega}^2 \mathbf{M} + j\boldsymbol{\omega} \mathbf{C} + \mathbf{K})^{-1} \mathbf{F}(\boldsymbol{\omega}). \tag{8}$$

FRF of the host beam and the metastructure is calculated using Eq. (8) and the bandgap frequency range is studied in the subsequent sections. The next section discusses the SDOF formulation of the Kalimba key resonators which will be attached to the host beam to study frequency selectivity.

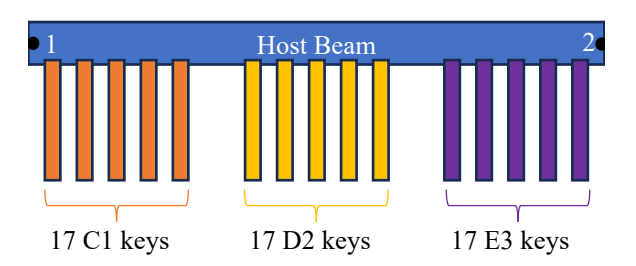


**FIGURE 2**. 17 keys each of C1, D2 and E3 keys arranged sequentially to the host beam.

## 3 SDOF FORMULATION OF KALIMBA KEY RES-ONATORS

To demonstrate the frequency selectivity in the Kalimbainspired metastructure, three sets each of 17 C1, 17 D2, and 17 E3 Kalimba keys are studied. The key notation is followed from that of standard Kalimba notation. Each of these sets is placed at a different spatial location on the host beam. Figure 2 shows a schematic of the metastructure and the spatial locations of the keys are given in Table 1. The key sets are arranged in the increasing order of natural frequencies. This ensured that the waves of lower frequencies were attenuated first and waves of higher frequencies were attenuated later. This ensures frequency selectivity and replication of BM behavior. Based on the changes in bandgap frequency ranges for each set of keys, the frequencies of the elastic waves attenuated will be analyzed. The Kalimba

Key Set	Natural Frequency (Hz)	Mass (g)	Spatial location (mm)
C1	261.6	2.9	101.6-511.0
D2	293.6	2.1	536.6-946.0
E3	329.6	2	971.6-138.10

**TABLE 1**. Natural frequencies, mass, and spatial locations of key sets.

keys are formulated as SDOF spring-mass systems attached to the host beam as shown in Figure 3. From the Kalimba instrument documentation, the frequencies at which each of the C1, D2, and E3 keys are tuned are known and are given in Table 1. The spring stiffness and the mass of the key need to be determined from the known natural frequency. The mass of the key was measured physically and was noted. The stiffness of the key

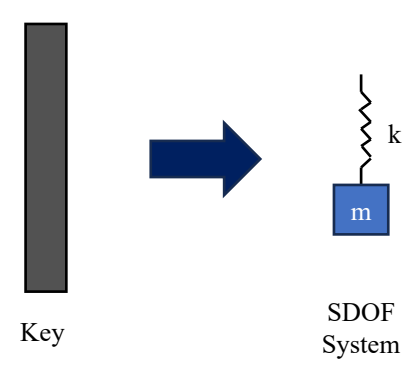


**FIGURE 3**. Each key is modelled as SDOF system whose mass and stiffness are determined using optimization.

can be calculated from the well-known formula of natural frequency,

$$\omega_n = \sqrt{\frac{k}{m}},\tag{9}$$

where  $\omega_n$  is the natural frequency in rad/s, k is the spring stiffness in N/m and m is mass of the key in kg. However, Eq. (9) will result in the correct stiffness value only when there is no uncertainty in tuning the Kalimba keys. Any uncertainty in the tuning of the keys will result in incorrect stiffness values. As there are 17 keys of a single type in one set, tuning each key exactly to the frequency given in Table 1 is unlikely in experiments and, therefore, will involve uncertainty. This uncertainty must be considered before formulating a model close to the real-world dynamics. To factor in this uncertainty, a vector of 17 different natural frequencies was considered for one particular set, one natural frequency each for one key. For a particular set of keys, the natural frequencies were close to those given in Table 1 for the corresponding set. To generate this vector, the 'randn' command in MATLAB with a mean value of the natural frequency given in Table 1 for a particular key set and a standard deviation of 1 was used. Once the vector for natural frequency is generated, the mass and stiffness of each key are determined from the natural frequency iteratively. The optimization problem for the same can be given as

minimize 
$$|\omega_n - \omega_c|$$
  
subject to  $0.5m_1 \le m \le 1.5m_1$ , (10)  
 $\omega_n^2 \times 0.5m_1 \le k \le \omega_n^2 \times 1.5m_1$ ,

where  $\omega_n$  is a natural frequency from the vector of natural frequencies,  $m_1$  is the mass of one of the keys measured physically,

and  $\omega_c$  is the natural frequency calculated for every iteration. The optimization given by Eq. (10) is performed using 'fmincon' command in MATLAB. Once the mass and stiffness are determined for each key, they are incorporated into the mass and stiffness matrices of Eq. (3), and the FE model for the metastructure is formulated. The next section discusses the formation of band gaps and frequency selectivity for different key sets.

## 4 BANDGAP FORMATION AND FREQUENCY SELEC-TIVITY

The response of the metastructure, and hence the frequency selectivity, is calculated for the case when each of the sets C1, D2, and E3 is attached to the beam separately and when all three sets are attached together. Figure 4 shows the transfer point FRF (displacement response measured at location '2' in Figure 2 with force at location '1') for the case when the C1 key set is attached to the beam. Figure 4 also shows the FRF transfer point for a beam without any attached keys. From Figure 4, an amplitude

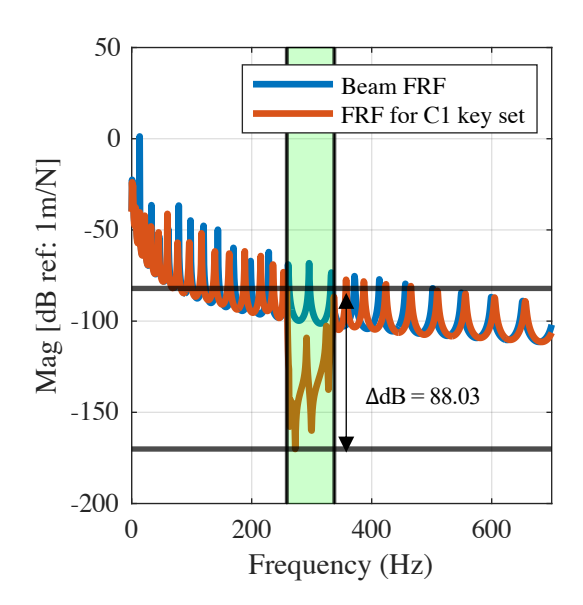


**FIGURE 4.** FRF for C1 key set shows a bandgap between 258.56-337.74 Hz and an amplitude drop of 88.03 dB.

drop of 88.03 dB can be seen in the frequency range 258.56-337.74 Hz signifying a bandgap region. This implies that any wave of a frequency in the bandgap frequency range will be attenuated. The transfer point FRF for the case when D2 keys are attached is shown in the Figure 5 and that for the case when E3 keys are attached are shown in the Figure 6. Bandgap regions can be identified from each case and the bandgap frequency ranges are summarized in the Table 2. From Table 2 it can be

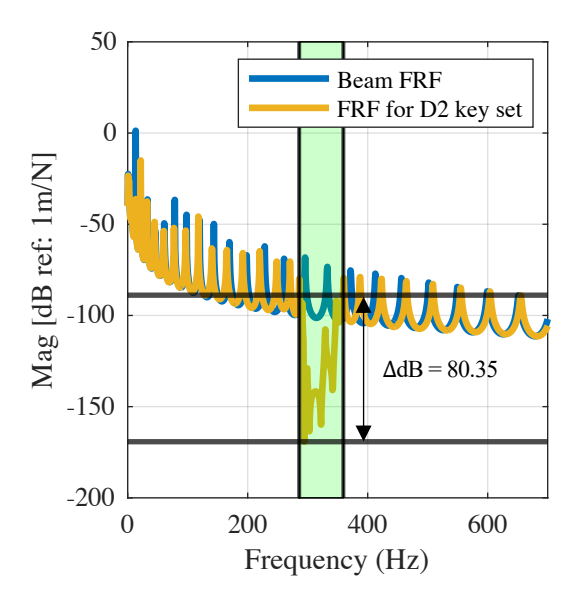


**FIGURE 5**. FRF for D2 key set shows a bandgap between 285.89-359.46 Hz with an amplitude loss of 80.35 dB

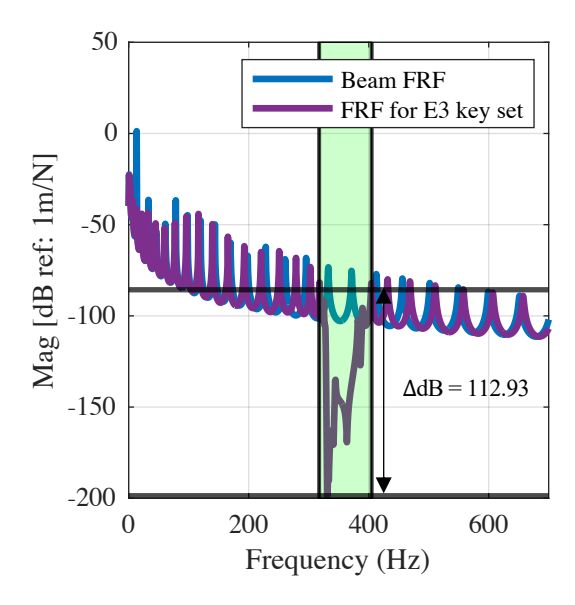


**FIGURE 6**. FRF for E3 key set shows a bandgap between 317.42-405 Hz with an amplitude loss of 112.93 dB

seen that the bandgap ranges shift towards higher values as keys of higher notes are used. This change in bandgap region by attaching different sets of keys indicates frequency selectivity.

An interesting phenomenon is observed when different sets of keys are attached sequentially to the beam and FRF is calculated for combined sets of keys. Figure 7 shows the transfer point FRF for the cases when only C1 keys are attached, when

Key Set	Bandgap Frequency Range (Hz)
C1	258.56-337.74
D2	285.89-359.46
E3	317.42-405
C1, D2	258.56-359.46
C1, D2, & E3	258.56-405

**TABLE 2**. Natural frequencies, mass, and spatial locations of key sets.

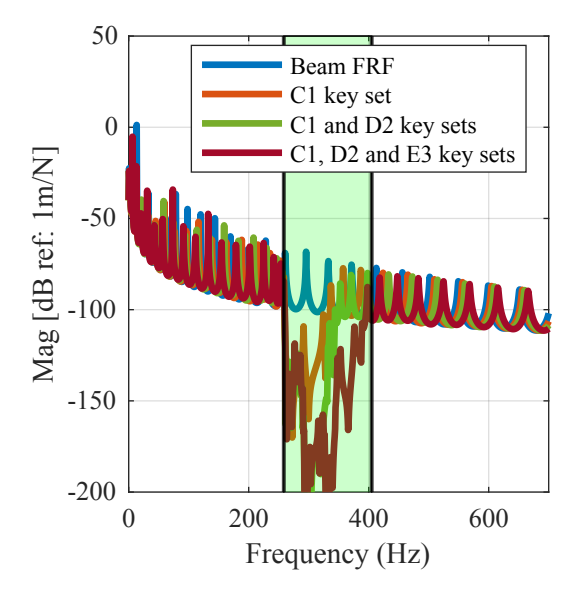


**FIGURE 7**. FRFs for the case when three key sets are attached to the beam sequentially shows combined bandgap effect of individual key sets.

C1 and D2 keys are attached and when C1,D2 and E3 keys are attached. It can be observed that as key sets are added, the combined bandgap effect of each key set occurs and the width of the bandgap region increases, thus providing more attenuation. The bandgap ranges of each of these cases have been summarized in Table 2. This finding is in line with the findings for locally resonant beams in [33]. Following the sequential addition of C1, D2, and E3 key sets, 5 more key sets of the higher notes were attached to the beam and the transfer point FRF for the case of 8 total key sets i.e. 136 keys was calculated. This FRF is shown in Figure 8. From Figure 8, it can be observed that the bandgap region now has increased to 258.56-613.11 Hz thus attenuating waves of a wider frequency range than before. These results demonstrate the efficacy of a Kalimba-inspired locally resonant ABM beam in enhancing frequency selectivity and thus in hearing restora-

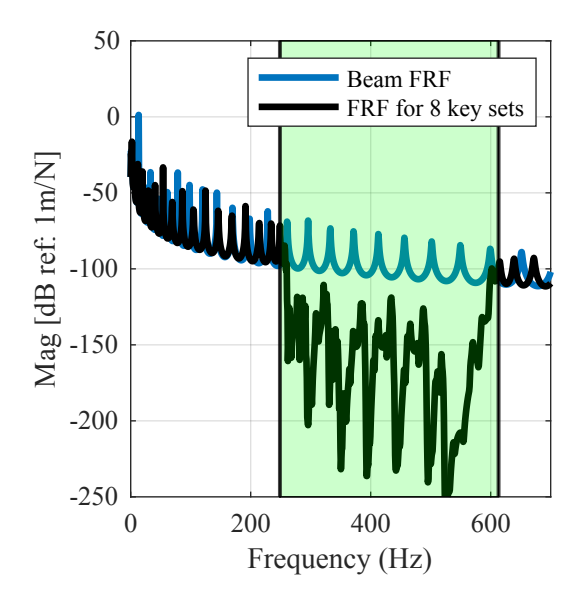


**FIGURE 8.** FRF for 8 key sets shows a bandgap between 258.56-613.11 Hz

tion. The bandgap and hence the frequency selectivity can thus be controlled by attaching different key sets on the host beam.

## 5 CONCLUSION

In this study, a novel design for an Artificial Basilar Membrane based on a locally resonant metastructure was proposed. In a simulated environment, Kalimba keys, acting as hair cells, were attached as resonators to a host beam and the response of the system was calculated. The FRF of the system exhibited a bandgap frequency region indicating attenuation of waves in a specific frequency region. The bandgap frequency region was found to change based on the type of the key set (C1, D2, and E3) attached to the beam. This demonstrated the attenuation of waves in different frequency regions, thus establishing frequency selectivity. Following this, the key sets were attached to the beam sequentially and the response of the system was calculated. It was found that as key sets were added, the bandgap width increased thus exhibiting wave attenuation in a wider frequency range. Lastly, eight key sets were attached to the beam sequentially, and the calculated response of the system demonstrated a bandgap region considerably wider than that for the prior cases of three key sets.

The design proposed in this study thus leverages the bandgap properties of the metastructures to replicate the frequency selectivity behavior of a Basilar Membrane. The results show a strong potential of the Kalimba-inspired metastructure for effective hearing restoration treatments. In addition, as frequency selectivity is found to change with a change in attached

Kalimba keys, the proposed design can be easier to tune to the needs of an individual as compared to the conventional ABM. The future work of this study includes the study of frequency selectivity through experimentation and scaling down of the proposed design to fit human ear.

#### **6 ACKNOWLEDGEMENT**

The authors would like to thank the support of the National Science Foundation through the grant CMMI-2301776 for sponsoring the research presented in this paper.

## **REFERENCES**

- [1] Hrncirik, F., Roberts, I., Sevgili, I., Swords, C., and Bance, M., 2023. "Models of cochlea used in cochlear implant research: a review". *Annals of Biomedical Engineering*, *51*(7), pp. 1390–1407.
- [2] Davaria, S., Malladi, V. V. S., Motaharibidgoli, S., and Tarazaga, P. A., 2019. "Cochlear amplifier inspired twochannel active artificial hair cells". *Mechanical Systems* and Signal Processing, 129, pp. 568–589.
- [3] Davaria, S., Sriram Malladi, V., and Tarazaga, P. A., 2019. "Bio-inspired nonlinear control of artificial hair cells". In Structural Health Monitoring, Photogrammetry & DIC, Volume 6: Proceedings of the 36th IMAC, A Conference and Exposition on Structural Dynamics 2018, Springer, pp. 179–184.
- [4] Wagner, E. L., and Shin, J.-B., 2019. "Mechanisms of hair cell damage and repair". *Trends in neurosciences*, **42**(6), pp. 414–424.
- [5] Carlyon, R. P., and Goehring, T., 2021. "Cochlear implant research and development in the twenty-first century: a critical update". *Journal of the Association for Research in Otolaryngology*, 22(5), pp. 481–508.
- [6] Boisvert, I., Reis, M., Au, A., Cowan, R., and Dowell, R. C., 2020. "Cochlear implantation outcomes in adults: A scoping review". *PLoS One*, *15*(5), p. e0232421.
- [7] Wilson, B. S., and Dorman, M. F., 2008. "Cochlear implants: current designs and future possibilities". *J Rehabil Res Dev*, **45**(5), pp. 695–730.
- [8] Kim, Y., Kim, J.-S., and Kim, G.-W., 2018. "A novel frequency selectivity approach based on travelling wave propagation in mechanoluminescence basilar membrane for artificial cochlea". *Scientific reports*, 8(1), p. 12023.
- [9] Chircov, C., and Grumezescu, A. M., 2022. "Microelectromechanical systems (mems) for biomedical applications". *Micromachines*, *13*(2), p. 164.
- [10] Jang, J., Jang, J. H., and Choi, H., 2017. "Biomimetic artificial basilar membranes for next-generation cochlear implants". Advanced healthcare materials, 6(21), p. 1700674.

- [11] Jang, J., Kim, S., Sly, D. J., O'leary, S. J., and Choi, H., 2013. "Mems piezoelectric artificial basilar membrane with passive frequency selectivity for short pulse width signal modulation". *Sensors and Actuators A: Physical*, **203**, pp. 6–10.
- [12] Jang, J., Lee, J., Woo, S., Sly, D. J., Campbell, L. J., Cho, J.-H., O'Leary, S. J., Park, M.-H., Han, S., Choi, J.-W., et al., 2015. "A microelectromechanical system artificial basilar membrane based on a piezoelectric cantilever array and its characterization using an animal model". *Scientific reports*, 5(1), p. 12447.
- [13] Dutta, A., 2006. "Proc. intern. mech. eng. congress and exposition". ASME Chicago, USA.
- [14] Heredia, A., Ambrosio, R., Moreno, M., Zuñiga, C., Jiménez, A., Monfil, K., and de la Hidalga, J., 2012. "Thin film membrane based on a-sige: B and mems technology for application in cochlear implants". *Journal of non-crystalline solids*, *358*(17), pp. 2331–2335.
- [15] Bachman, M., Zeng, F.-G., Xu, T., and Li, G.-P., 2006. "Micromechanical resonator array for an implantable bionic ear". *Audiology and Neurotology*, *11*(2), pp. 95–103.
- [16] Xu, T., Bachman, M., Zeng, F.-G., and Li, G.-P., 2004. "Polymeric micro-cantilever array for auditory front-end processing". *Sensors and Actuators A: Physical*, 114(2-3), pp. 176–182.
- [17] voN BékésY, G., 1970. "Travelling waves as frequency analysers in the cochlea". *Nature*, **225**(5239), pp. 1207–1209.
- [18] Von Békésy, G., 1960. "Experiments in hearing.".
- [19] Chadwick, R., Fourney, M., and Neiswander, P., 1980. "Modes and waves in a cochlear model". *Hearing research*, 2(3-4), pp. 475–483.
- [20] Xia, A., Visosky, A. M. B., Cho, J.-H., Tsai, M.-J., Pereira, F. A., and Oghalai, J. S., 2007. "Altered traveling wave propagation and reduced endocochlear potential associated with cochlear dysplasia in the beta2/neurod1 null mouse". *Journal of the Association for Research in Otolaryngology*, 8, pp. 447–463.
- [21] Cook, L. P., and Holmes, M., 1981. "Waves and dispersion relations for hydroelastic systems". *SIAM Journal on Applied Mathematics*, **41**(2), pp. 271–287.
- [22] White, R. D., and Grosh, K., 2005. "Microengineered hydromechanical cochlear model". *Proceedings of the National Academy of Sciences*, *102*(5), pp. 1296–1301.
- [23] Tanaka, K., Abe, M., and Ando, S., 1998. "A novel mechanical cochlea" fishbone" with dual sensor/actuator characteristics". *IEEE/ASME transactions on mechatronics*, 3(2), pp. 98–105.
- [24] Shintaku, H., Kobayashi, T., Zusho, K., Kotera, H., and Kawano, S., 2013. "Wide-range frequency selectivity in an acoustic sensor fabricated using a microbeam array with non-uniform thickness". *Journal of Micromechanics and*

- Microengineering, 23(11), p. 115014.
- [25] Kim, S., Song, W. J., Jang, J., Jang, J. H., and Choi, H., 2013. "Mechanical frequency selectivity of an artificial basilar membrane using a beam array with narrow supports". *Journal of Micromechanics and Microengineering*, 23(9), p. 095018.
- [26] Jeon, H., Jang, J., Kim, S., and Choi, H., 2018. "Characterization of a piezoelectric aln beam array in air and fluid for an artificial basilar membrane". *Electronic Materials Letters*, *14*, pp. 101–111.
- [27] Liu, Y., and Zhang, X., 2011. "Metamaterials: a new frontier of science and technology". *Chemical Society Reviews*, **40**(5), pp. 2494–2507.
- [28] Matlack, K. H., Bauhofer, A., Krödel, S., Palermo, A., and Daraio, C., 2016. "Composite 3d-printed metastructures for low-frequency and broadband vibration absorption". *Proceedings of the National Academy of Sciences*, 113(30), pp. 8386–8390.
- [29] El-Borgi, S., Fernandes, R., Rajendran, P., Yazbeck, R., Boyd, J., and Lagoudas, D., 2020. "Multiple bandgap formation in a locally resonant linear metamaterial beam: Theory and experiments". *Journal of Sound and Vibration*, 488, p. 115647.
- [30] Chavan, S. H., Malladi, S. S., and Malladi, V. V. S., 2023. "Reinforcement learning approach of switching bi-stable oscillators to adapt bandgaps of 1d-meta-structures". *Me-chanical Systems and Signal Processing*, 191, p. 110151.
- [31] Valipour, A., Kargozarfard, M. H., Rakhshi, M., Yaghootian, A., and Sedighi, H. M., 2022. "Metamaterials and their applications: an overview". *Proceedings of the Institution of Mechanical Engineers, Part L: Journal of Materials: Design and Applications,* 236(11), pp. 2171–2210.
- [32] Graff, K. F., 2012. *Wave motion in elastic solids*. Courier Corporation.
- [33] Chavan, S. H., 2023. "Programming the bistable dynamic vibration absorbers of a 1d-metastructure for adaptive broadband vibration absorption". PhD thesis, Michigan Technological University.